

RSC Advances



This is an *Accepted Manuscript*, which has been through the Royal Society of Chemistry peer review process and has been accepted for publication.

Accepted Manuscripts are published online shortly after acceptance, before technical editing, formatting and proof reading. Using this free service, authors can make their results available to the community, in citable form, before we publish the edited article. This *Accepted Manuscript* will be replaced by the edited, formatted and paginated article as soon as this is available.

You can find more information about *Accepted Manuscripts* in the [Information for Authors](#).

Please note that technical editing may introduce minor changes to the text and/or graphics, which may alter content. The journal's standard [Terms & Conditions](#) and the [Ethical guidelines](#) still apply. In no event shall the Royal Society of Chemistry be held responsible for any errors or omissions in this *Accepted Manuscript* or any consequences arising from the use of any information it contains.

CuInSe₂ thin film solar cells prepared by low-cost electrodeposition techniques from non-aqueous bath

Priyanka U. Londhe, Ashwini B. Rohom and Nandu B. Chaure*

Department of Physics, Savitribai Phule Pune University (formerly University of Pune),
Pune-411007, INDIA

Polycrystalline CuInSe₂ (CIS) thin films have been prepared by low-cost electrochemical method from non-aqueous ethylene glycol solvent onto cadmium sulfide (CdS) thin films. The co-deposition potential for Cu, In and Se was optimized with cyclic voltammetry measurements. CIS layers were electrodeposited at -1.1, -1.3 and -1.5 V versus Ag/AgCl references in air-tight custom made electrodeposition cell. The films were selenized at 400 °C for 20 minutes. The optical, structural, morphological, compositional and optoelectronic properties of as-prepared and selenized samples were studied using UV-Vis spectrophotometer, X-ray diffractometer, Transmission electron microscopy (TEM), Scanning electron microscope (SEM), Energy dispersive x-ray analysis (EDAX) and current-voltage (I-V) measurements. Three prominent sharp peaks of tetragonal CIS, (112), (204)/(220), and (312/116) were revealed in all as-prepared and selenized samples. Upon selenization the crystallinity of the samples was found to be improved remarkably. Compact, void free, and nearly uniform thin films of grain size ~ 1 μm were deposited. The as-deposited and selenized CIS samples were Cu-rich whereas the contents of Se was ~ 50% obtained by EDAX analysis. The value of inter-planer distance, $d = 3.339 \text{ \AA}$ was measured by HRTEM corresponds to (112) plane of tetragonal CIS crystal structure. The circular spotted rings observed in selected area diffraction (SAD) pattern were confirmed (112), (204)/(220) and (312)/(116) reflections of CIS. The solar cell parameters, V_{oc} , J_{sc} , FF and efficiency were found to be 303 mV, 28 mA/cm² and FF ~ 53 % and $\eta = 4.5 \%$ for the CIS film deposited at -1.5 V. The values of shunt conductance, $G_D = 2.5 \text{ mS/cm}^2$ and $G_L = 7.9 \text{ mS/cm}^2$ and series resistance, $R_D = 0.81 \text{ } \Omega\text{cm}^2$ and $R_L = 0.19 \text{ } \Omega\text{cm}^2$ were calculated for dark and illuminated conditions. Mott-Schottky analysis is also carried out on the final solar cell in dark and illuminated condition to study the carrier concentration and defects in the CdS/CIS interface.

Keyword: CuInSe₂, Thin film solar cells, Electrodeposition, Non-aqueous bath, crystallinity,

***Corresponding author Email-** n.chaure@physics.unipune.ac.in

Tel No. +91 20 2569 9072; Fax No.: +91 20 2569 1684.

INTRODUCTION

The chalcopyrite I-III-VI₂ compounds have been the topic of intense research in recent years. Polycrystalline CuInGaSe₂ (CIGS) have emerged as a leading material in thin film solar cell technology due to their applicability as absorber materials for highly efficient and cost effective solar electricity generation. Ideally, the absorber material of an efficient terrestrial photovoltaic cell should have a direct energy band gap in the range 1.2-1.5 eV, high optical absorption coefficient, and long diffusion length of minority carriers, which is fulfilled by CIGS. Solar cells based on CIGS fabricated by vacuum evaporation technique are currently leading in terms of conversion efficiency around 21.7% in laboratory scale¹. CIS and CIGS can be deposited using vacuum deposition techniques like sputtering², co-evaporation³, flash evaporation⁴, molecular beam epitaxy⁵, pulsed laser deposition⁶ and stacking elemental layers⁷, which are reasonably expensive due to the capital investment and use of highly pure source materials. Highly crystalline with controlled stoichiometric binary, ternary and quaternary semiconductor thin films can be prepared by vacuum techniques, however the technical issues such as deposition over large area, slow deposition rate, are unresolved. A non-vacuum technique such as, spray paralysis⁸, chemical bath deposition (CBD)⁹, sol-gel and electrodeposition (ED)¹⁰⁻¹³ have also been used successfully for the preparation of CIS thin films. Electrodeposition is one of the low-cost techniques to deposit semiconductor/metal films over large area with high deposition rate. The controlled stoichiometry can be maintained in the precursor layer by electrochemical deposition¹⁴. One step, multi-step, pulsed, stacked layer electrodeposition techniques are commonly adapted to prepared CIS, CIGS and CZTS chalcopyrite thin films¹⁵⁻²⁰. The power conversion efficiency 7.0 % is reported by Qiu et al²¹ using one-step electrodeposition from aqueous bath. A non-aqueous electrolyte can be used to deposit semiconductor, oxide and insulator thin films, which allows depositing layer at higher growth potentials which can be limited in aqueous medium due to hydrogen evolution. Besides this the layers can be deposited for higher bath temperature to enhance the homogeneity, crystallinity and particle size. There have been a very few reports available on the electrodeposition of CIS from non-aqueous medium²²⁻²⁴. Bhattacharya et al²² has reported the basic studies on the growth of CIGS from dimethyl sulfoxide (DMSO). Dharmadasa et al.²² have used ethylene glycol as a solvent to electrodeposit CIS thin film however, they have not reported the development solar cells. Nevertheless, the

similar electrolyte had been used previously in the literature to prepare the CdTe²⁵, CdHgTe²⁶ and CdZnTe²⁷ material and their solar cell.

In the present studies we have potentiostatically electrodeposited CIS thin films from non-aqueous (ethylene glycol) bath onto cadmium sulfide thin films and investigated the effect of deposition potential on optical, structural, morphology and composition properties of CIS layer have been discussed. The as-prepared CIS layers electrodeposited from ethylene glycol at high bath temperature (130 °C) are highly crystalline with large grains as compare to the layers prepared from aqueous bath ²⁸. The reported procedure could be helpful to produce the low-cost solar cell devices on plastic (flexible) substrate.

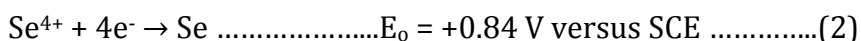
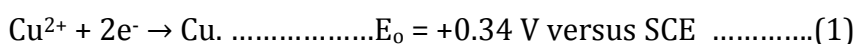
EXPERIMENTAL DETAILS

CIS thin films were potentiostatically electrodeposited in ethylene glycol onto CdS substrates at 130 °C using Biologic potentiostat/galvanostat model SP150. CdS thin films were prepared by chemical bath deposition method on fluorine doped tin oxide (FTO) coated glass substrates. The detailed study is reported elsewhere ²⁹. Prior to cyclic voltammetry (CV) and deposition of CIS, CdS layers were annealed at 400 °C for 20 min. A conventional three-electrode geometry with Ag/AgCl as reference, FTO as working and graphite as counter electrode were used. CuCl₂, InCl₃ and SeCl₄ purchased from Sigma- Aldrich of purity at least 99.9 % were used as received. LiCl was used as a supporting chemical compound to control the ionic conductivity of bath. Three different potentials, -1.1, -1.3 and -1.5 V versus Ag/AgCl reference optimized by CV measurement were chosen to electrodeposit CIS thin films. The temperature of bath was maintained at 130 °C during CV measurements and growth of thin films without agitation. The samples were selenized in a home-made selenization chamber at 400 °C for 20 min. Selenized CdS/CIS samples were etched in Br-methanol and NaCN solution to remove the unwanted secondary phases of Cu and Se. Finally, a circular Au contact of area 3 mm diameter were made by vacuum evaporation technique. The structural properties of films were studied by X-ray diffractometer, Model Bruker D8, with CuK α radiation of wavelength 1.5405 Å. The presence of crystallographic planes and inter-planner distance was measured directly with the help of transmission electron microscopy (TEM) model, TECNAI G². The film morphology was examined using JEOL JSM-6360A Scanning electron microscopy (SEM) at accelerating voltage 20 kV and

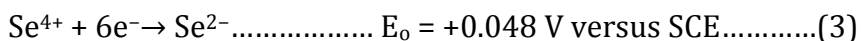
probe current 1 nA. The EDAX attachment available in above SEM instrument was employed to obtain the compositional analysis. The optical properties were studied by using JASCO UV-Vis-NIR spectrophotometer. I-V and C-V measurement were performed using Biologic Potentiostat attached with probe station and necessary software. The optoelectronic properties of complete solar cell device were measured under illumination with power intensity 100 mW/cm² at room temperature ~ 25 °C. Incident-photon-to-current conversion efficiency (IPCE) was measured by photoncounting spectrometer, ISS Inc., and Kiethley 2400 source meter.

RESULTS AND DISCUSSION

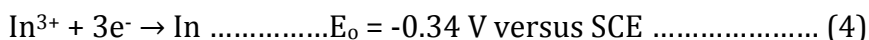
CV measurement was carried out to investigate the electrochemical processes during electrodeposition of CuInSe₂ in the range 0 V to -2.0 V versus Ag/AgCl reference electrode. The cyclic voltammogram recorded with scan 10 mV sec⁻¹ on CdS substrate without agitation is depicted in figure 1. Cathodic and anodic scans are marked by forward and reverse arrows, respectively. CV measurement was begun at 0 V to avoid the stripping of CdS layer, therefore the initial feature related to the reduction of Cu and Se have not been observed. A cathodic current was initially found to be increased could be due to the elemental deposition of Cu and/or Se by the following charge transfer reaction;



and/or



A plateau region observed up to -0.7 V is proposed due to the deposition of Cu_xSe_y compounds. Indeed, we have observed that the films electrodeposited in this region were brownish in color with powdery deposition. Further the cathodic current rises with increasing the cathodic potential due to the deposition of In along with Cu and Se by following charge transfer reaction,



An exponential increase in cathodic current beyond -1.0 V could be due to the co-deposition of Cu, In and Se. A sharp rise in the current around -1.0 V and higher cathodic potential was not

observed, which confirms the absence of hydrogen evolution in non-aqueous bath. Note that we have not observed any bubbling from the cathode for higher cathodic potential up to -1.8 V versus Ag/AgCl. During anodic scan three different shoulder's observed at \sim -1.40 V, -0.85 V and -0.30 V are assigned for the stripping of In and Cu deposited at over potential depositions. The stripping peak of Se was not observed, which would be expected at lower cathodic potentials (+ve potential). As the clear plateau region was not observed in cyclic voltammogram, therefore, the CIS thin films have been electrodeposited at three different potentials -1.1 V, -1.3 V and -1.5 V versus Ag/AgCl onto CdS substrate.

The XRD pattern of as-prepared and selenized CIS films electrodeposited at -1.1 V, -1.3 V and -1.5 V on CdS substrate is depicted in figure 2 A) and B), respectively.

Highly polycrystalline CIS thin films preferentially oriented along (112) plane are obtained for all growth potentials. Three prominent peaks corresponds to (112), (204)/(220) and (312)/(116) reflection are observed in as-prepared samples. A wider base observed in as-prepared CIS sample deposited at -1.1 V for reflections (112) and (204/220) is due to the presence of secondary phases of Cu_2Se_3 (JCPDS Card No. 72-1421) marked as solid square (\blacksquare). The reflections associated to FTO are marked as solid circle (\bullet). CIS sample electrodeposited at -1.5 V on to CdS substrate was found to be highly crystalline without secondary phases of Cu_xSe_y . Upon selenization the peak corresponds to CdS (101) reflection (JCPDS Card No. 41-1041) was attributed at $2\theta = 28.20^\circ$. The crystallinity of as-prepared CIS thin films deposited for -1.3 V and -1.5 V in non-aqueous bath is much higher than the annealed CIS samples prepared in aqueous bath²⁸. Therefore, the electrodeposition of CIS in non-aqueous bath may be useful for the development of solar cell on flexible substrates without heat treatment or selenization.

The secondary peaks associated to Cu_xSe_y were not attributed after selenization in all samples grown at different potentials. An enhancement in the crystallinity of CIS peak was further observed upon selenization. The full width at half maximum (FWHM) calculated for (112) peak was found to be decreased substantially from 0.51° , 0.36° and 0.30° to 0.30° , 0.15° and 0.12° for the sample grown at -1.1 V, -1.3 V and -1.5 V, respectively. The enhancement in the crystallinity with selenization at higher temperature is proposed due to the re-crystallization of material along with the agglomeration of small grains.

The surface topographical images of as-prepared and selenized samples were recorded using the scanning electron microscope (SEM), Model- JEOL JSM-6360A. Figure 3 a), b) and c) are the SEM images of as-prepared CIS thin films deposited at potentials -1.1 V, -1.3 V and -1.5 V on to CdS substrates. The corresponding selenized images are depicted in figure 3 d), e) and f), respectively. The physical appearance of the samples was grayish-black in color with well adherent to the substrate.

SEM images are clearly shows a void free deposition of CIS alloy over large area. The globular surface morphology of grain size ranging from ~ 500 nm to $1.5 \mu\text{m}$ was observed in the sample deposited at -1.1 V, whereas the mixed surface morphology consisting spherical particles as well as long niddle like structure can be seen for the samples deposited at -1.3 V. Overgrowth of the particle of size $\sim 4\text{-}5 \mu\text{m}$ was observed for the sample deposited at -1.5 V. The overgrowth of the particle is associated to the mass-transfer coefficient. The large overgrowth is due to the higher deposition rate of diffusion limiting species. The deposition time for all samples was kept 30 minute. Diffused uniform grains can be clearly seen upon selenization. The enhancement observed in the grain is associated to the re-crystallization of material. The compositional analysis of as-prepared and selenized CIS thin films deposited for -1.1 V, -1.3 V and -1.5 V were obtained by EDAX. All as-prepared samples were Cu-rich and the content of Se was nearly similar close to 50 atomic percentages. After selenization the atomic percentage concentration of Cu was found to be reduced and nearly stoichiometric CIS thin films are obtained at -1.5 V growth potential. The Cu/In ratio was systematically decreased for selenized sample from 2.09 to 1.34 with increasing the cathodic potential. The elemental composition (atomic percentage) obtained by EDAX analysis is tabulated in table 1.

Figure 4 shows the plots of $(\alpha h\nu)^2$ versus energy ($h\nu$) for CIS thin films deposited for -1.1 V, -1.3 V and -1.5 V versus Ag/AgCl reference. The optical band gap was found to be in the range of 1.06 eV to 1.01 eV (± 0.05) and 0.98 eV to 0.95 eV (± 0.05) for as-deposited and selenized samples, respectively. The band gap estimated for as-deposited and selenized sample was nearly similar within an error ± 0.05 . Sharp fundamental absorption edge could be seen upon selenization. This could be due to the re-crystallization of thin films along with the homogeneous phase formation. The values of the band-gap estimated from the optical absorption spectra are summarized in table 2.

Figure 5 shows the HRTEM (a) and SAD pattern (b) of the selenized CIS thin film deposited at -1.5 V. The 'd' spacing obtained by HRTEM analysis is 3.339 Å, which corresponds to (112) reflection of tetragonal structure of CIS. Three dotted circular rings correspond to (112), (204)/(220) and (312)/(116) planes of CIS are observed in selected area diffraction pattern. This is in good agreement with the structural data obtained by XRD.

The film deposited at -1.5 V shows good optical and structural properties. Moreover, the stoichiometric CIS layers were obtained upon selenization. Therefore, we have studied the optoelectronic properties of CdS/CIS solar cell wherein CIS was electrodeposited at -1.5 V versus Ag/AgCl reference electrode. The most common tool for solar cell analysis is the current-voltage (J-V) measurements under standard illumination 100 mW/cm² (AM 1.5). The J-V measurement results four solar cell parameters, short circuit current (J_{sc}), open circuit voltage (V_{oc}), fill factor (FF) and power conversion efficiency (η), which are often used to characterize the photovoltaic device. J_{sc} depends on the absorption of photons and collection of carriers, whereas V_{oc} is ruled by the band gap of the absorber and the degree of recombination in the cell. These parameters are well accepted indicators of solar cell performance and are particularly valuable for comparing and qualifying cells.

The J-V behavior of a thin film solar cell (TFSC) can be described by a general single exponential diode equation³⁰,

$$J = J_0 \exp \left[\frac{q}{nkT} (V - RJ) \right] + GV - J_L \dots \dots \dots (5)$$

where R, the series resistance, and G shunt conductance that occur in series or parallel with the primary diode, respectively.

The behavior of device and diode parameters were studied with the plots of J-V, dJ/dV versus V and dV/dJ versus $(J+J_{sc})^{-1}$, each comparing the data measured under dark and illumination conditions. Figure 6 shows the current-voltage graph of CIS solar cell under dark and illuminated condition. The values of solar cell parameters (J_{sc} , V_{oc} , FF and η) obtained from graph 6 are summarized in table 3. The cross-over observed between the dark and illuminated I-V curve, which is commonly seen in TFSC. This may be due to the defect states present in the absorber or at the hetero-interface or in the CdS layer³¹⁻³⁴. The stability of the absorber material (CIGS) can

be further improved by optimizing the selenization parameters, which will not only prevent the crossover but also improve the solar cell performance.

Some non-ideal effects, such as current blocking behavior or light-to-dark crossover in forward bias or breakdown in reverse bias commonly observed in TFSCs are not explained by the J-V curve. The plots of dJ/dV versus V , dV/dJ versus $(J+J_{sc})^{-1}$ are derived from the J-V curves in dark and illuminated condition. The diode term in the equation (5) becomes negligible for the plot dJ/dV against V (figure 7) near J_{sc} and in reverse bias. If the shunt term is ohmic and J_L is constant, $g(V)$ will be flat with the value in reverse bias equal to G . The values of G for dark and illuminated condition is found to be $G_D = 2.5 \text{ mS/cm}^2$ and $G_L = 7.9 \text{ mS/cm}^2$, respectively.

A plot of dV/dJ against $(J+J_{sc})^{-1}$ yield a straight line if J_L is independent of voltage. A linear fit to the data gives an intercept to y-axis and slope are equivalent to series resistance 'R' and ideality factor 'n'. The values of series resistance, R_D and R_L and ideality factor, n_D and n_L deduced from figure 8 a) and b) under dark and illuminated condition, respectively are given table 3. The suffix 'D' and 'L' indicates the parameters calculated for dark and illuminated condition of solar cell. Generally, the ideality factor is ~ 2 when the recombination current dominates and ~ 1 when the diffusion current dominates which determined for the forward bias current at lower potential region. The values of n_D and n_L have been found between 1 and 2 indicates both currents are comparable³⁵.

The IPCE measurement of the above solar cell device was performed and results are depicted in figure 9. The CIS cell exhibited a high response to visible light in the wavelength 450-600 nm. However, in the near-infrared wavelength region the IPCE response was poor. The loss in the IPCE for higher wavelength (<600 nm) region could be due to the thin (1.5-2 μm) CIS absorber layer. Thin absorber layer directly affect the absorption coefficient, which gives rise to the incomplete generation of electron-hole pair in CIS layer³⁰. The other reason for the loss in QE in the above region may be the trap states (defects) present in the bulk CIS layer, which leads to the recombination of electrons and holes.

CV measurement on diode is normally analyzed using the depletion approximation. According to this approximation the capacitance response of the junction originates solely from the edge of the depletion region which means that the junction is modeled as a plate capacitor.

For an ideal abrupt homo-junction diode the inverse of the capacitance is given by

$$1/C^2 = \frac{2}{q\epsilon_s A^2 N} (V_{bi} - V) \dots\dots\dots (6)$$

where, q is the unit charge, ϵ_s the static permittivity of semiconductor, V_{bi} the built-in voltage and V the applied voltage. The value of ϵ_s is calculated by considering the dielectric constant of material, $\epsilon_r = 13.5$ ³⁶ and the permittivity of free space, ϵ_0 .

Ideally, it yields a straight line whose intersect with the voltage axis gives the junction built in potential and slope determines the acceptor concentration of the absorber material. The figure 10 a) and b) represents the Mott-Schottky plots for CdS/CIS thin film solar cell device measured under dark and illuminated conditions, respectively. The calculated values of carrier density in dark (N_{AD}) and illuminated (N_{AL}) condition are consistent with reported values for CIS prepared by various methods^{12, 37-39}. As expected the higher carrier density was obtained upon illumination of solar cell. These values are tabulated in table 3. Capacitance under illumination was found to be increased could be due to the trapping of photo generated charge carriers at the irrelevant states within the band gap.

CONCLUSION

Highly polycrystalline chalcopyrite CIS thin films have been electrodeposited from non-aqueous bath on CdS substrates for higher cathodic potentials (~ 1.5 V) versus Ag/AgCl reference electrode. This process could be effective for the electrodeposition of CIGS thin films, where the deposition of Ga is difficult along with Cu, In and Se. Selenization procedure not only support to enhance the crystallinity but also helped to obtained nearly stoichiometric CIS films. The sharp fundamental absorption edge with energy gap $\sim 0.98 (\pm 0.05)$ eV was estimated from selenized CIS thin films. Compact, well adherent and void free CIS layers were electrodeposited for all reported potentials. The dotted circular rings correspond to (112), (204)/(220) and (312)/(116) planes of tetragonal CIS are revealed in SAD pattern. The inter-planer distance 'd' obtained by HRTEM corresponds to (112) reflection of CIS. The solar cell parameters, V_{oc} , J_{sc} , FF and efficiency were found to be 303 mV, 28 mA/cm² and FF ~ 53 % and $\eta = 4.5$ % for the CIS film deposited at -1.5 V. The values of shunt conductance, $G_D = 2.5$ mS/cm² and $G_L = 7.9$ mS/cm² and series resistance, $R_D = 0.81$ Ω cm² and $R_L = 0.19$ Ω cm² were calculated for dark and

illuminated conditions. The increased capacitance observed in Mott-schottky plot upon illumination may be due the presence of trap states (defects) within the material or at the interface.

ACKNOWLEDGMENTS

The authors would like to thank the Defence research and development organization (DRDO), New Delhi, India (ERIP/ER/10003866/M/01/1388) for providing the financial support under major research grant.

REFERENCES

1. M. A. Green, K. Emery, Y. Hishikawa, W. Warta and E. D. Dunlop, *Prog. Photovolt. Res. Appl.*, 2015, **23**, 1-9.
2. R. Ingrid, A. C. Miguel, E. Brian, B. Egaas, C. DeHart, J. Scharf, C.L. Perkins, B. To, R. Noufi, *Prog. Photovolt. Res. Appl.*, 2008, **16**, 235-239.
3. A. H. Moharram, M. M. Hafiz, A. Salem, *Appl. Surf. Sci.*, 2001, **172**, 61-67.
4. A. Ashida, Y. Hachiuma, N. Yamamoyo, Y. Cho, *J. Mater. Sci. Lett.*, 1994, **13**, 1181-1184.
5. S. Niki, A. Yamada, R. Hunger, P.J. Fonsa, K. Iwataa, K. Matsubara, A. Nishiob, H. Nakanishi, *J. Cryst Growth* 2002, **237-239**, 1993-1999.
6. X. L. Wang, G. J. Wang, B. L. Tian, Z. L. Du, *Chin. Sci. Bull.*, 2010, **55**, 1854-1858.
7. A. N. Tiwari, M. Krejci, F. J. Haug, H. Zogg, *Prog. Photovolt. Res. Appl.*, 1999, **7**, 393-397.
8. T. Terasako, Y. Uno, T. Kariya, S. Shirakata, *Sol Energy Mater Sol Cell.*, 2006, **90**, 262-275.
9. H. M. Pathan, C. D. Lokhande, *Appl. Surf. Sci.*, 2005, **245**, 328-334
10. H. Lee, W. Lee, J. Kim, M. Ko, K. Kim, K. Seo, D. Lee, H. Kim, *Electrochim. Acta.*, 2013, **87**, 450-456
11. R. N. Bhattacharya, *J. Electrochem. Soc.*, 1983, **130**, 2040-2042.
12. N. B. Chaure, A. P. Samantilleke, R. P. Burton, J. Young, I. M. Dharmadasa, *Thin Solid Films*, 2005, **472**, 212-216.

13. X. Donglin, X. Man, L. J. Zhuang, Z. Xiujian, *J. Mater. Sci.*, 2006, **41**,1875-1878.
14. N. B. Chaure, J. Young, A.P. Samantilleke, I.M. Dharmadasa, *Sol. Energy Mater. Sol. Cells.*, 2004, **81**, 125–133.
15. J. Tao, J. Liu, J. He, K. Zhang, J. Jiang, L. Sun, P. Yang and J. Chu, *RSC Adv.*, 2014,**4**, 23977-23984
16. J. Tao, K. Zhang, C. Zhang, L. Chen, H. Cao, J. Liu, J. Jiang, L. Sun, P. Yang and J. Chu, *Chem. Commun.*, 2015, **51**,10337-10340
17. J. C. Malaquias, D. Regesch, P. J. Dale, M. Steichen, *Phys. Chem. Chem. Phys.*, 2014, **16**, 2561
18. Ashwini B. Rohom & Priyanka U. Londhe & N. B. Chaure, *J Solid State Electrochem.*,2015, 19,201-210
19. M. Lakhe and N. B. Chaure, *Sol. Energy Mater. Sol. Cells.*, 2014, **123**, 122–129
20. P. U. Londhe, A. B. Rohom, N. B. Chaure, *J Mater Sci: Mater Electron* (2014) 25:4643–4649
21. S.N. Qiu, L. Li, C.X. Qiu, I. Shih, C.H. Champness, *Sol. Energy Mater. Sol. Cells*, 1995, **37** 389-393
22. R.N. Bhattacharya, M.A. Contreras, J. Keane, A.L. Tennant, J.R. Tuttle, K. Ramanathan, R. Noufi, US Patent 5 804 054, 1998.
23. J. S. Wellings, A. P. Samantilleke, S. N. Heavens, P. Warren, I. M. Dharmadasa, *Sol. Energy Mater. Sol. Cells.*, 2009, **93**, 1518–1523.
24. N. B. Chaure, *J. Renew. Sustainable Energy*, 2013, **5**, 0316041-7.
25. R. K. Pandey, S. Maffi, and L. P. Bicelli, *Mater. Chem. Phys.*, 1993, **35**, 15-20.
26. J. P. Nair, R. Jayakrishnan , N. B. Chaure, S. Gohkale, A. Lobo, S.K. Kulkarni, R.K. Pandey, *J. Phys. & Chem. Solids* 1999, **60**, 1693–1703
27. N. B. Chaure, S. Chaure, R. K. Pandey, *Electrochimica Acta* 2008, **54**, 296–304
28. N. B. Chaure, J. Young, A.P. Samantilleke, I.M. Dharmadasa, *Sol. Energy Mater. Sol. Cells.*, 2004, **81**, 125–133.
29. N. B. Chaure , S. Bordas , A. P. Samantilleke , S. N. Chaure , J. Haigh , I. M. Dharmadasa, *Thin Solid Films*, 2003, **437**, 10–17.
30. S. S. Hegedus, W. N. Shafarman, *Prog. Photovolt: Res. Appl.*, 2004, **12**, 155–176.

31. M. Nichterwitz, R. Caballero, C. A. Kaufmann, H.W. Schock, T. Unold, J. Appl. Phys., 2013, **113**, 044515-4.
32. A. O. Pudov, A. Kanevce, H. A. Al-Thani, J. R. Sites, and F. S. Hasoon, J. Appl. Phys., 2005, **97**, 064901-2.
33. I. L. Eisgruber, J. E. Granata, J. R. Sites, J. Hou, J. Kessler, Sol. Energy Mater. Sol. Cells, 1998, **53**, 367—377.
34. K. B. Messaoud, M. Buffière, G. Brammertz, H. ElAnzeery, S. Oueslati, J. Hamon, B. J. Kniknie, M. Meuris, M. Amlouk, J. Poortmans, Prog. Photovolt: Res. Appl., (2015)
35. S. M. Sze, Physics of Semiconductor Devices, Jonh Wiley and sons, Inc. (1993)
36. S. Ouédraogo, F. Zougmore, J. M. Ndjaka, International Journal of Photoenergy, Volume 2013, Article ID 421076, 9 pages <http://dx.doi.org/10.1155/2013/421076>
37. S. M. Hasan, M. A. Subhan, K. M. Mannan, Optical Materials, 2000, **14**, 329-336.
38. B. J. Stanbery, Critical Reviews in Solid State and Materials Sciences, 2002, **27(2)**, 73–117.
39. K. Bindu, C. S. Kartha, K. P. Vijayakumar, T. Abe, Y. Kashiwaba, Sol. Energy Mater. Sol. Cells, 2003, **79**, 67–79.

Figure Captions

Figure 1. A typical cyclic voltammogram recorded in an electrolyte consisting ionic species CuCl_3 , InCl_3 and SeCl_4 , with scan rate 10 mV/sec at temperature 130 °C using Ag/AgCl reference electrode on CdS substrate. LiCl was used as supporting chemical compound to control the ionic conductivity of bath.

Figure 2. X-ray diffractogram of the CIS thin film deposited at -1.1 V a), -1.3 V b) and -1.5 V c), A] As-prepared and B] Selenized XRD spectra of the CIS layers deposited at above growth potentials.

Figure 3. SEM images of as-prepared a), b) and c) and the corresponding selenized d), e) and f) CIS films electrodeposited on at -1.1 V, -1.3 V and -1.5 V, respectively

Figure 4. Optical absorption spectra recorded for as-deposited and selenization a), b) and c) CIS thin film deposited on CdS at -1.1 V, -1.3 V and -1.5 V, respectively.

Figure 5. a) HRTEM image of selenized CIS layer deposited at -0.5 V and the corresponding b) selected area diffraction (SAD) pattern

Figure 6. Dark and illuminated J-V curves of CdS/CIS heterostructure solar cell device. CIS layer was electrodeposited at -1.5 V versus Ag/AgCl reference electrode.

Figure 7. A graph of dJ/dV vs V for CdS/CIS heterostructure solar cell device. The experimental data depicted in figure 6 is processed to obtain these graphs.

Figure 8. A graph of dV/dJ vs $(J+J_{sc})^{-1}$ for CdS/CIS solar measured in dark a) and illuminated b) conditions. The experimental data depicted in figure 6 is processed to obtain these graphs.

Figure 9. Incident photon-to-current efficiency (IPCE) curve for superstrate (FTO/CdS/CIS/Au) structured solar cell.

Figure 10. Mott-Schottky, $1/C^2$ versus voltage plot for CdS/CIS thin film solar cell, a) dark and (b) illuminated condition recorded for frequency 50 kHz.

Table Caption

Table 1. A summary of compositional analysis of CuInSe_2 thin films electrodeposited on CdS substrate.

Table 2. A summary of band gap calculated for CuInSe_2 thin films deposited on FTO/CdS at various deposition potentials

Table 3. A solar cell parameters obtained under dark and illuminated conditions.

Table 1

Deposition potential Versus Ag/AgCl (V)	Composition (Atomic percentage)							
	Cu		In		Se		Cu/In ratio	
	As-deposited	Selenized	As-deposited	Selenized	As-deposited	Selenized	As-deposited	Selenized
1.1	36.10	35.81	22.00	17.10	41.91	47.10	1.64	2.09
-1.3	40.41	29.74	25.12	21.53	34.47	48.73	1.60	1.38
-1.5	35.13	28.62	26.46	21.30	38.41	50.09	1.33	1.34

Table 2

Deposition Potential (V)	Band gap (eV)	
	As-deposited	Selenized
-1.1 V	1.06 ± 0.05	0.98 ± 0.05
-1.3 V	1.03 ± 0.05	0.96 ± 0.05
-1.5 V	1.01 ± 0.05	0.95 ± 0.05

Table 3

Cell	V_{oc} (volts)	J_{sc} (mA/cm ²)	FF	η %	G_D (mS/cm ²)	G_L (mS/cm ²)	R_D Ω cm ²	R_L Ω cm ²	n_D	n_L	N_D cm ⁻³	N_L cm ⁻³
FTO/CdS/ CIS/Au	0.303	28	0.53	4.5	2.5	7.9	0.81	0.19	1.9	1.5	1.09* 10 ¹⁶	1.05* 10 ¹⁶

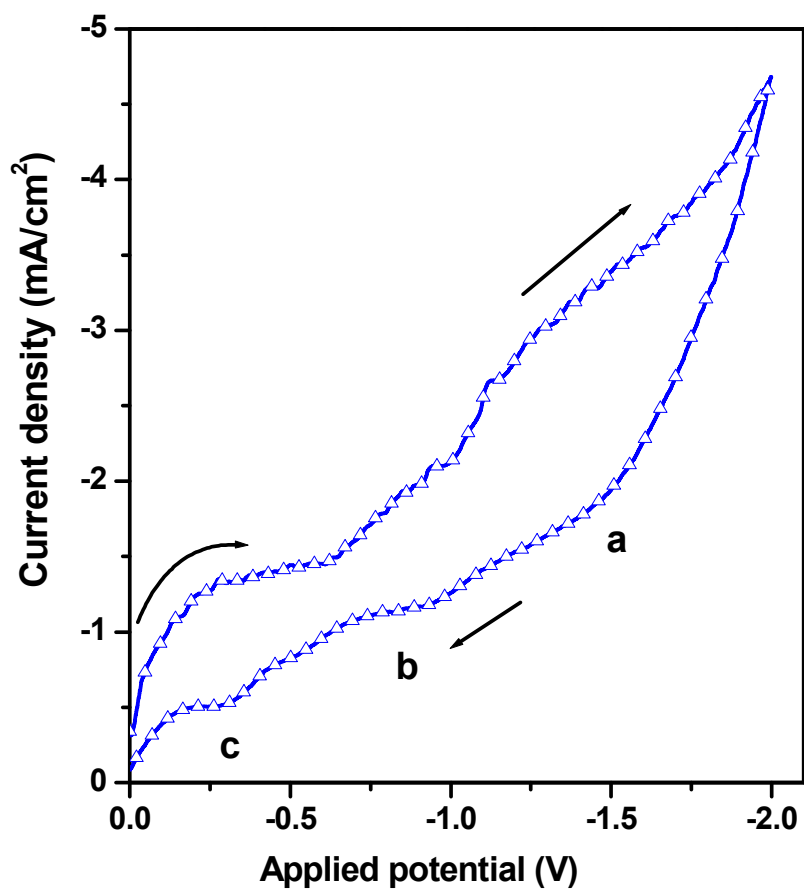


Figure 1. A typical cyclic voltammogram recorded in an electrolyte consisting ionic species CuCl_3^- , InCl_3 and SeCl_4 , with scan rate 10 mV/sec at temperature 130 °C using Ag/AgCl reference electrode on CdS substrate. LiCl was used as supporting chemical compound to control the ionic conductivity of bath.

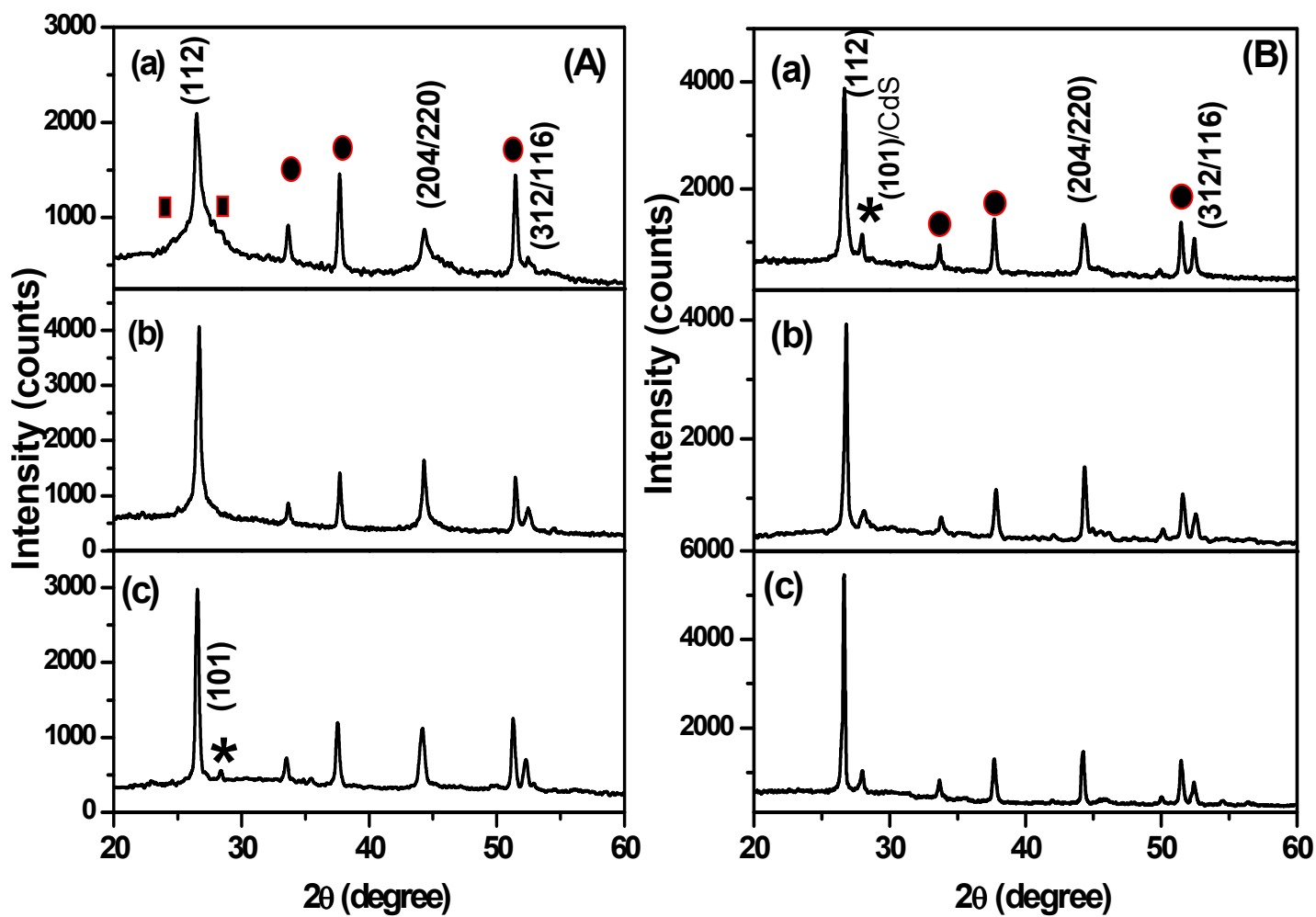


Figure 2. X-ray diffractogram of the CIS thin film deposited at -1.1 V a), -1.3 V b) and -1.5 V c), A] As-prepared and B] Selenized XRD spectra of the CIS layers deposited at above growth potentials.

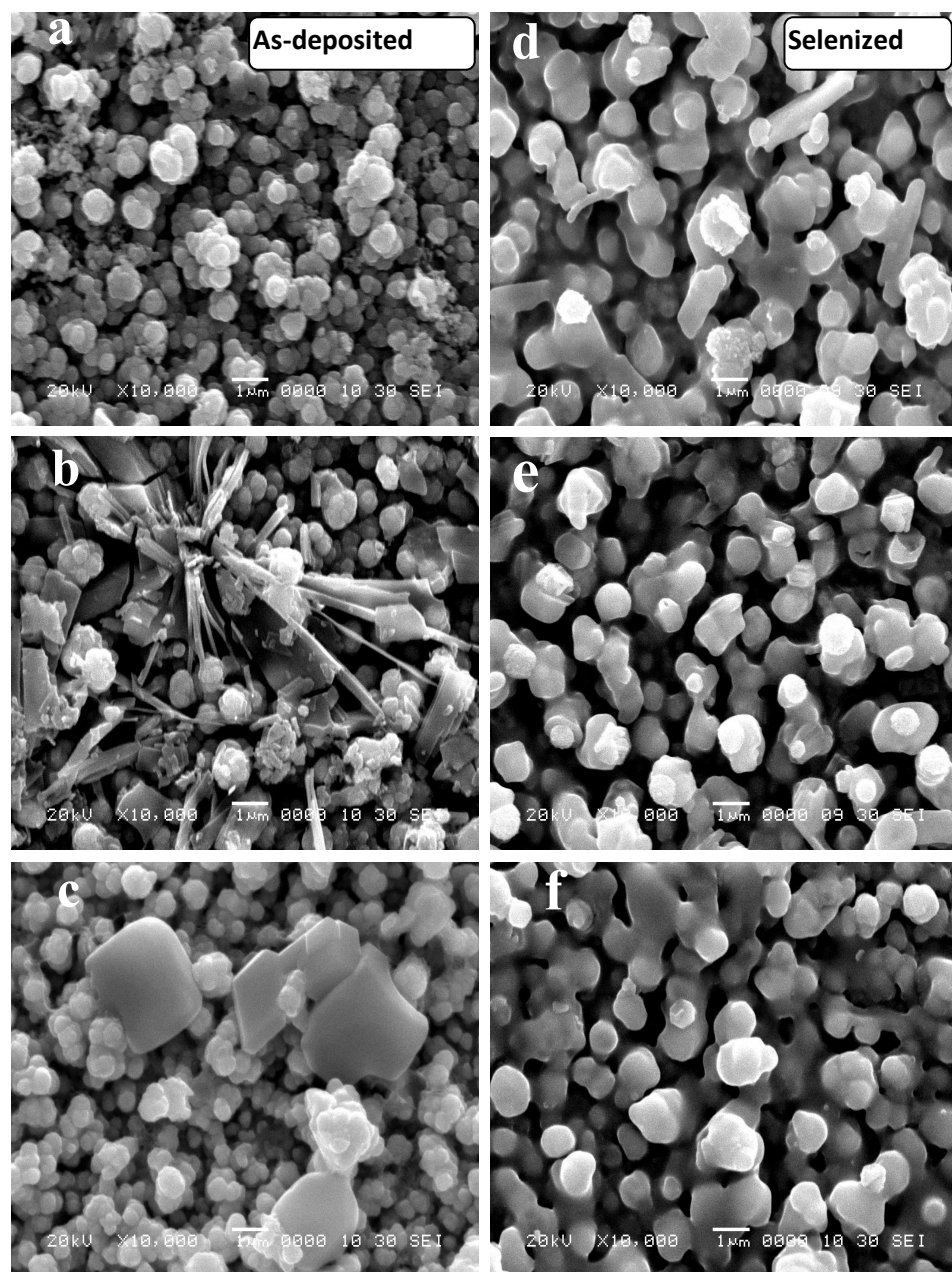


Figure 3 SEM images of as-prepared a), b) and c) and the corresponding selenized d), e) and f) CIS films electrodeposited on at -1.1 V, -1.3 V and -1.5 V, respectively

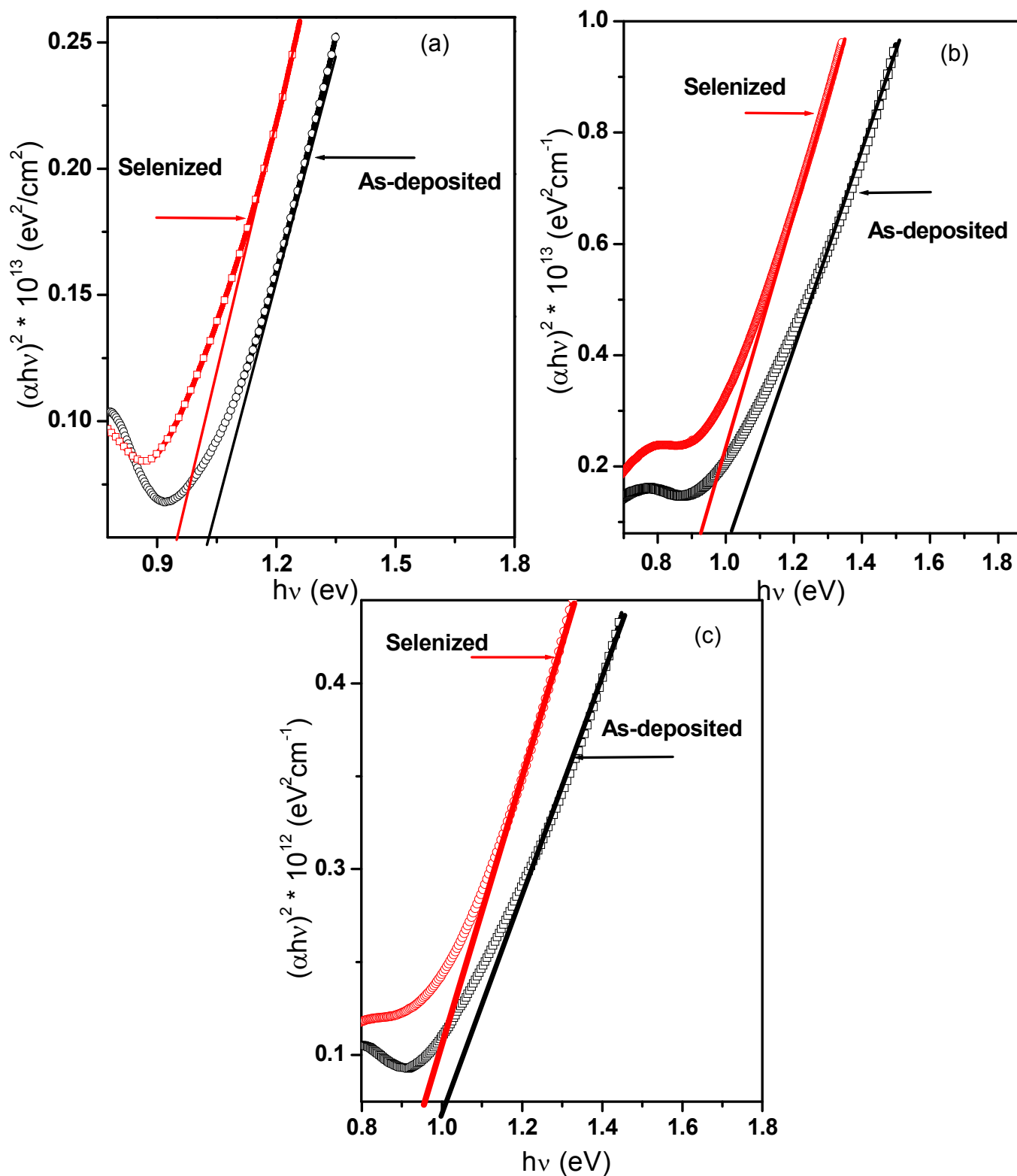


Figure 4 Optical absorption spectra recorded for as-deposited and selenization a), b) and c) CIS thin film deposited on CdS at -1.1 V, -1.3 V and -1.5 V, respectively.

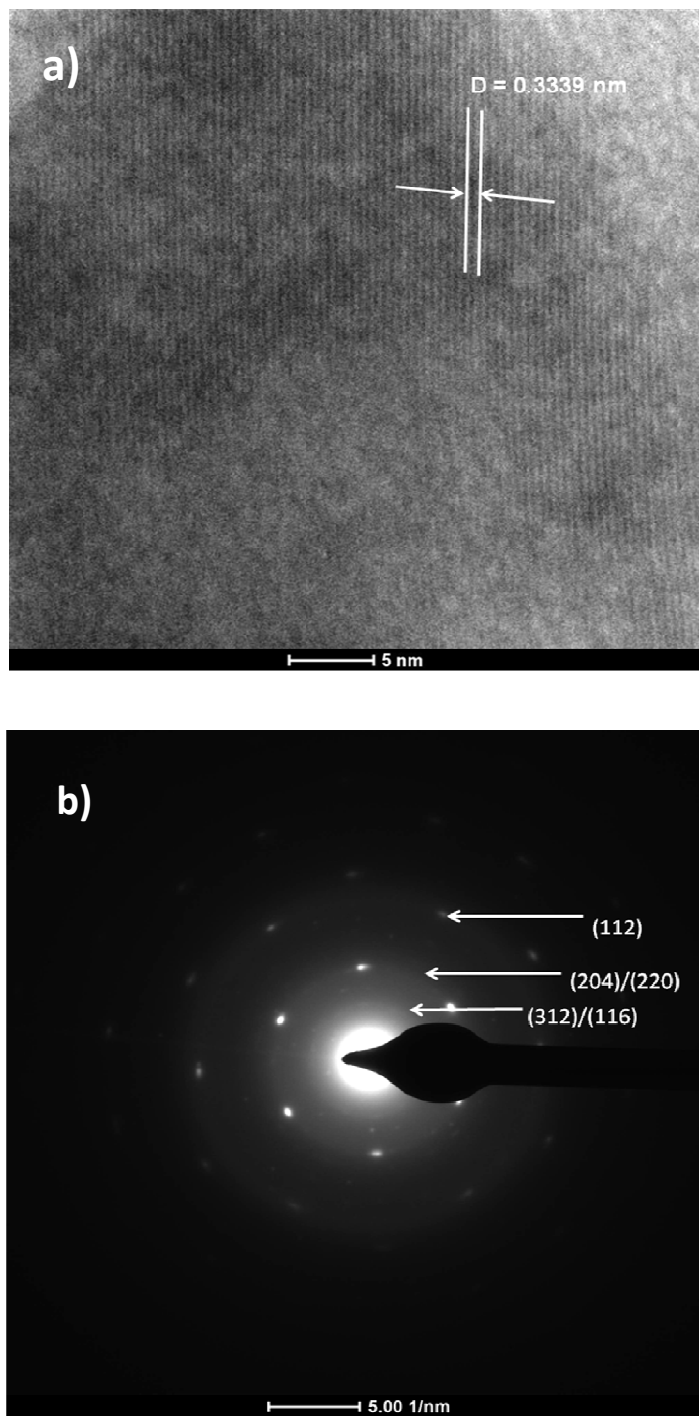


Figure 5 a) HRTEM image of selenized CIS layer deposited at -0.5 V and the corresponding b) selected area diffraction (SAD) pattern

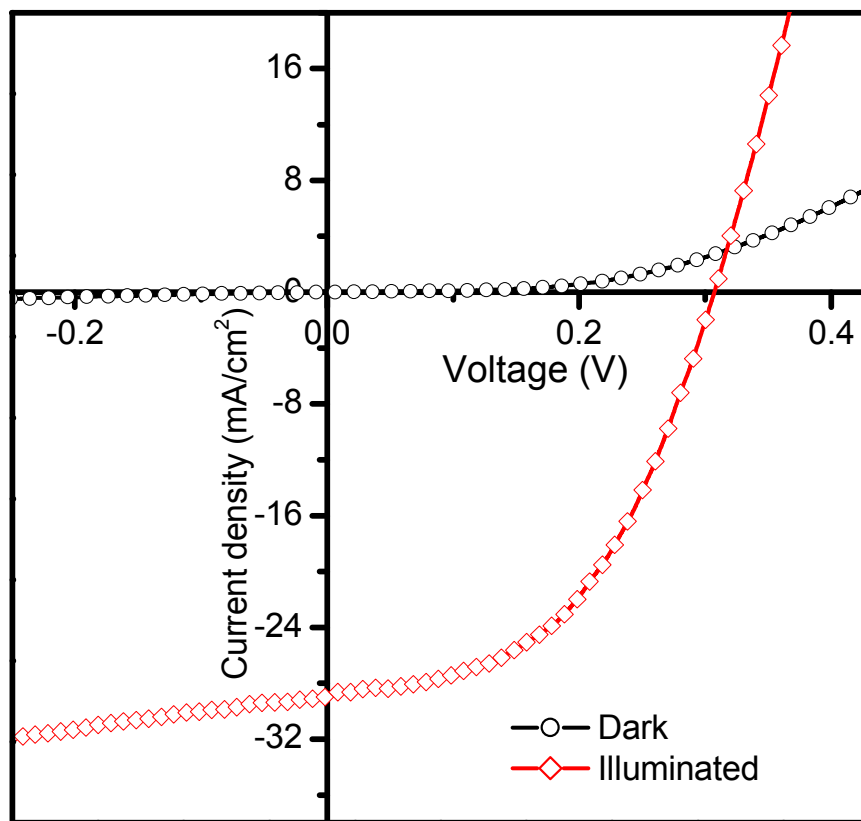


Figure 6 Dark and illuminated J-V curves of CdS/CIS heterostructure solar cell device. CIS layer was electrodeposited at -1.5 V versus Ag/AgCl reference electrode.

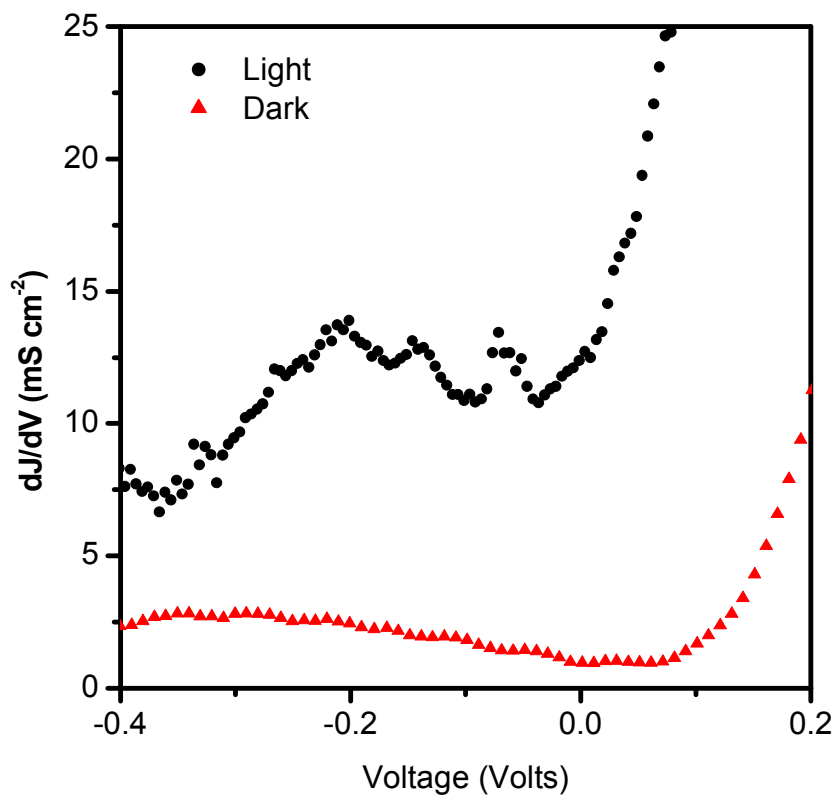


Figure 7 A graph of dJ/dV vs V for CdS/CIS heterostructure solar cell device. The experimental data depicted in figure 6 is processed to obtain these graphs.

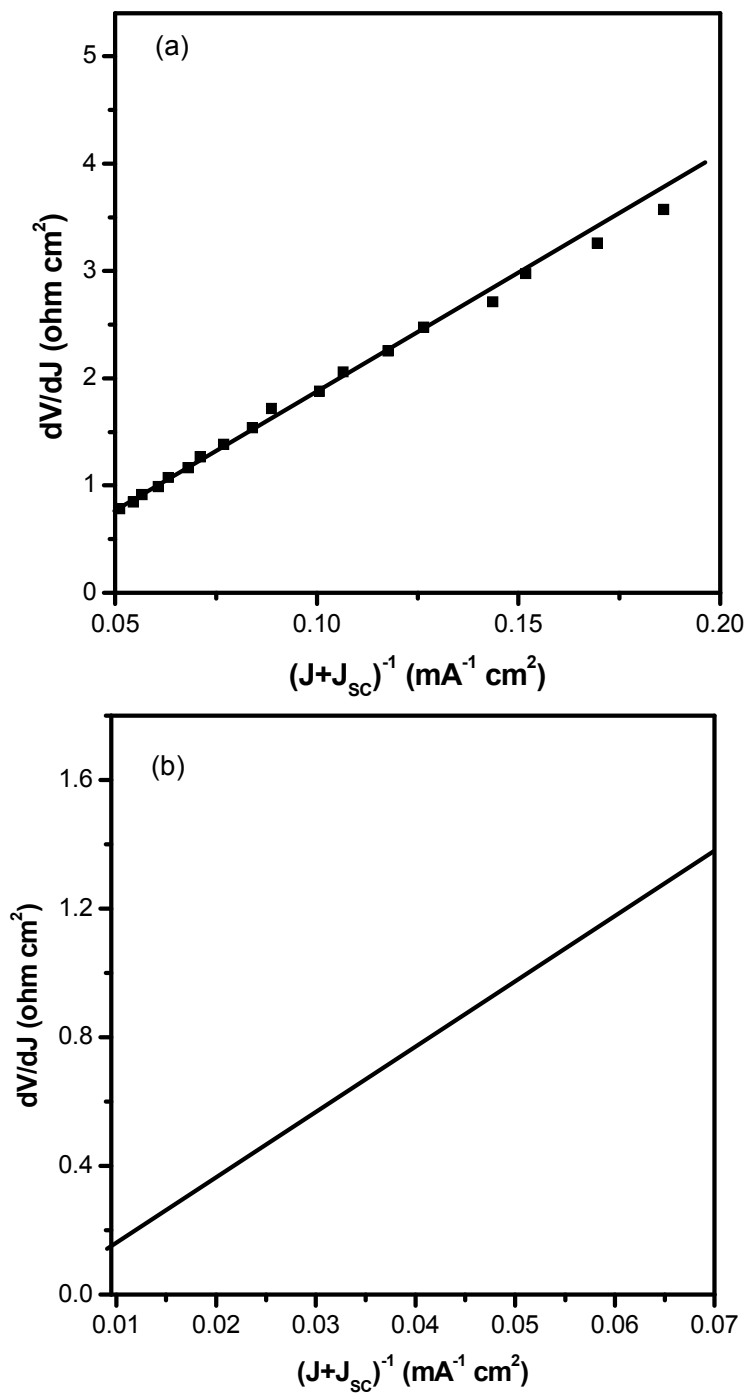


Figure 8 A graph of dV/dJ vs $(J+J_{sc})^{-1}$ for CdS/CIS solar measured in dark a) and illuminated b) conditions. The experimental data depicted in figure 6 is processed to obtain these graphs.

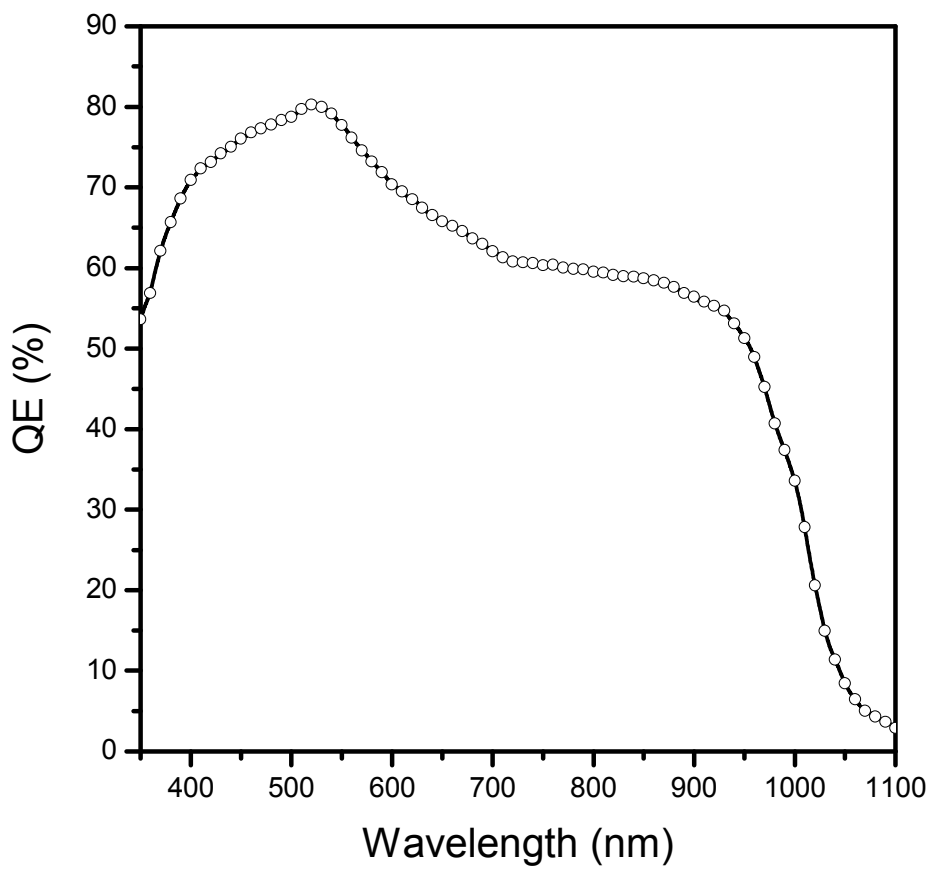


Figure 9. Incident photon-to-current efficiency (IPCE) curve for superstrate (FTO/CdS/CIS/Au) structured solar cell.

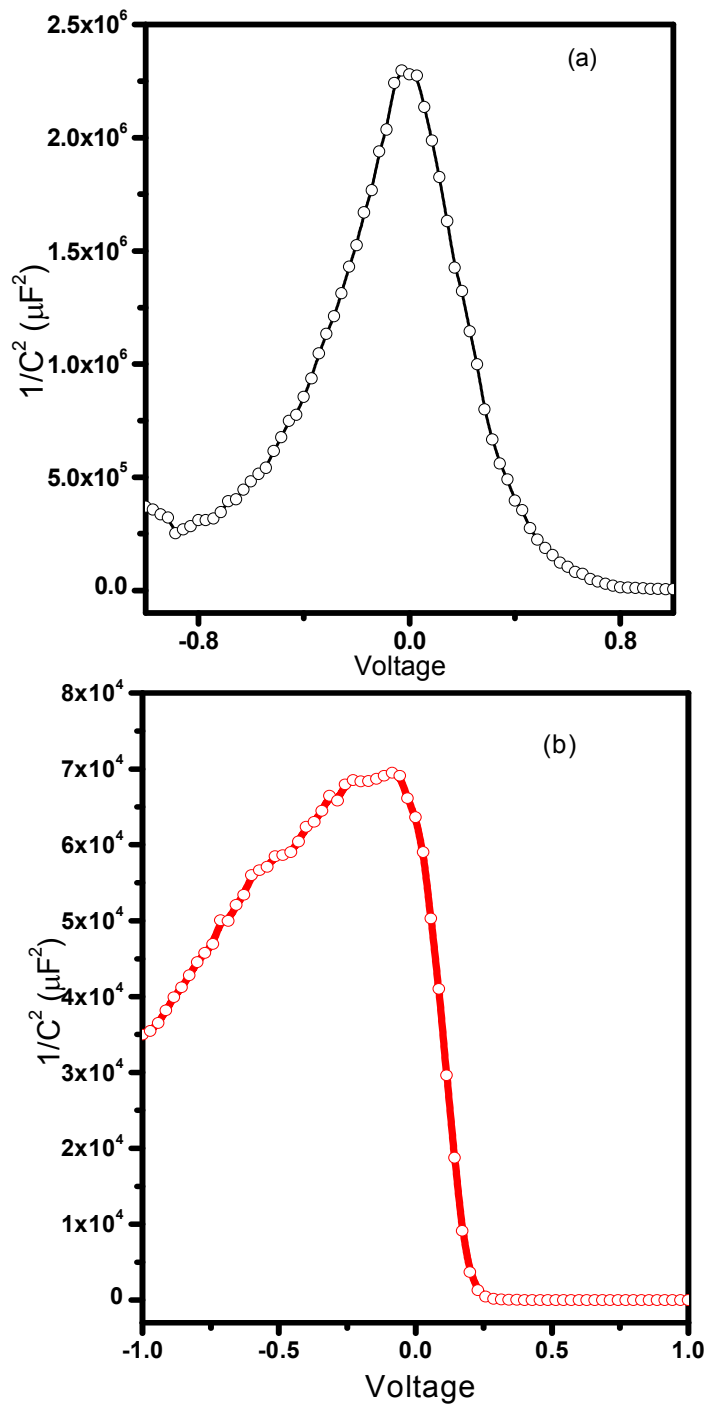


Figure 10 Mott-Schottky, $1/C^2$ versus voltage plot for CdS/CIS thin film solar cell, a) dark and (b) illuminated condition recorded for frequency 50 kHz.